Ab initio study of the electrostatic dipole modulation due to cation substitution in HfO_2/SiO_2 interfaces

A. G. Van Der Geest,[1,2] P. Blaise,[1] and N. Richard[2]
[1]*CEA, LETI, MINATEC, F-38054 Grenoble, France*
[2]*CEA, DAM, DIF, F-91297 Arpajon, France*

(Received 15 December 2011; revised manuscript received 18 May 2012; published 27 August 2012)

The interface between HfO_2 and SiO_2 is of much technological interest for complementary metal-oxide semiconductor (CMOS) technology in microelectronic devices. The valence band offset between HfO_2 and SiO_2 is a property of particular importance for this interface because it can be modulated by adding substitutional cations like Al, La, and Mg. We study the effects of these substitutional cations within this interface by using *ab initio* techniques in order to obtain the electrostatic dipole modulation and the corresponding change in the valence band offset in relation to dopant free reference HfO_2/SiO_2 interfaces. Al, La, and Mg are substituted for both Hf and Si atoms close to the interface during a detailed analysis of the dipole at the microscopic scale. This reproduces not only the experimental trends, but also demonstrates that the effects of the dopants are strongly dependent upon their positions and their chemical environments. Specifically, the modulation of the charge distribution by the dopants shows a complicated structure consisting of several peaks that contribute to the interfacial dipole centered around the oxygen atoms that bridge between the HfO_2 and the SiO_2. We also include a first-order G_0W_0 correction to recover band offset results compatible with the experimental values.

DOI: 10.1103/PhysRevB.86.085320 PACS number(s): 73.30.+y, 73.20.At, 73.21.Ac, 73.40.Ty

I. INTRODUCTION

In recent years, the microelectronics industry has begun transitioning the dielectric material in complementary metal-oxide semiconductor (CMOS) transistors from silicon dioxide to hafnium-based dielectrics such as HfO_2 or $HfSiO_x$ silicates.[1,2] The higher dielectric function provided by these high-κ materials allows for the continued reduction in size of transistors by maintaining sufficiently low tunneling currents. Nevertheless, this new class of dielectrics introduces unexpected complications. During thermal treatments, oxygen atoms diffuse toward the HfO_2/Si-substrate interface and grow a SiO_2 film.[3,4] Since this film is usually nonstoichiometric and induces a higher concentration of defects in the HfO_2, a thin SiO_2 layer of less than 1 nm is purposely grown between HfO_2 and Si to reduce the proportion of defects.[5] This thin layer preserves the high quality of the critical SiO_2/Si interface for electron conduction through a silicon channel.[6] As a consequence of increasing the number of material layers, the fine tuning of the threshold voltage of the entire gate stack is more difficult than before. One of the solutions considered consists of introducing dopants at the HfO_2/SiO_2 interface in order to tune the band offsets without modifying the global electronic properties of the stack.

Several types of dopants have recently been studied both theoretically and experimentally, including Al,[7–13] La,[7,10–14] Mg,[14,15] and Sr.[10] Of particular interest here are the dopants introduced through diffusion from capping layers of La, Al, or Mg containing materials.[7,9–11,14,15] Narayanan *et al.* reviewed the construction of high-κ gate *n*FETs and *p*FETs, discussing the inclusion of capping layers as an important means of controlling the threshold voltage,[14] while Bosman *et al.* recently studied the distribution of chemical elements within a HfO_2/SiO_2 gate stack from Al and La capping layers.[7] When these studies are coupled with the measurements of the valence band offset (VBO),[11] it shows that Al tends to decrease the VBO of HfO_2/SiO_2, while La increases it, but without any clear explanation of the intrinsic cause. Theoretically, Luo *et al.*[13] also confirm the direction of the VBO shifts in their investigation of the location of Al and La dopants within the interfaces. They have also discussed the modification of the electronic dipole by these dopants with a phenomenological model including the effect of electronegativity of the metal dopant.

The introduction of these dopants through diffusion coupled with the variation in growth processes introduces many possible combinations of nanoscopic arrangements that can be difficult to treat computationally. This issue has been recently called the variability issue.[16] Some studies have already focused on the variability issue for the SiO_2/Si interface.[17–19] While many studies have been directed towards the building of new gate stacks, the specific HfO_2/SiO_2 interface is only beginning to be well understood at the atomic scale, in relation to its structure and concerning the role of dopants.[2,8,12,13,20–24]

In order to render possible the theoretical study of the variability issue without including all possible structural factors that could be affected during the deposition processes or by the various thermal treatments, one has to carefully select the materials phases, interface orientations, chemistry of the interfaces, and dopants locations. As explained in detail in part III of this paper, we specifically deal with the variance of the orientation between monoclinic HfO_2 (m-HfO_2) and β-cristobalite SiO_2 (β-SiO_2) by constructing and calculating the VBO of low strain interfaces using *ab initio* methods. These interfaces are then used as a basis through which we study the inclusion of single dopants of Al, La, and Mg, with a particular attention devoted to the microscopic analysis of the dipole variations as a function of the different dopant locations.

II. CALCULATION METHODS

A. Parameters of DFT

All the density functional theory (DFT) calculations have been performed using a GGA-PBE[25] functional,

spin-polarized framework. The DFT calculations were primarily within the software code SIESTA,[26] which employs a computationally efficient (compared to plane waves) linear combination of atomic orbitals. This permits us to screen many possibilities for the orientations of surfaces and interfaces, and the location of dopants.

Careful convergence studies of the total Kohn-Sham energy and cell parameters were performed upon all the materials used to create our model interfaces or used as dopants: monoclinic HfO_2, β-cristobalite SiO_2, gaseous O_2, hexagonal close packed Mg, face center cubic Al, hexagonal close packed La, and hexagonal La_2O_3. The pseudopotentials used to describe each species were all of the Troullier-Martins[27] scheme with relativistic[28] and nonlinear core[29] corrections applied to Hf and La, with Mg using just the core correction.

The energy shift, mesh cutoff parameters, and the Brillouin zone sampling (k-points grid) were primarily selected to satisfy the numerical convergence of the total energy and cell parameters of monoclinic HfO_2 at an accuracy of less than 50 meV/atom and 0.1 Å, respectively. The basis set used was a polarized double-ζ basis (DZP) with an energy shift of 150 meV. A mesh cutoff of 325 Ry with an increased grid cell sampling was used for the self-consistent convergence of the electronic wave function with an electronic thermal smearing of 300 K (Fermi-Dirac distribution). The Monkhorst-Pack scheme[30] of $4 \times 4 \times 4$ was used for the k-point sampling of the bulk calculations and of $4 \times 4 \times 1$ for the surface and interface calculations. All geometry optimizations were performed using a conjugate gradient algorithm[26] with a force convergence tolerance of 0.04 eV/Å. The other non-HfO_2 systems were all shown to be converged within the parameters previously cited, which were selected to be the strictest required for the convergence of these materials.

B. G_0W_0 corrections

When DFT is used without any correction in its LDA or GGA form, the VBO of the HfO_2/SiO_2 interface deviates from experiment by up to a few electron volts, to the point that the valence band of SiO_2 can be above the one of HfO_2, in qualitative disagreement with experiment.[8,20,21,23] The many-body correction to DFT (G_0W_0) uses first-order response functions to correct the electronic levels for the many-body effects that are insufficiently calculated in DFT. By employing a G_0W_0 correction calculated for the bulk structures of two insulating materials that form an interface, several authors have shown the accuracy of this method in predicting not only accurate band gaps, but also the band edge locations and the corresponding band offsets with an error of a few tenths of electron volts.[24,31–34] The G_0W_0 correction can also be used to correct the location of the valence bands for insulators and the Fermi energy for metals in relation to the electrostatic potential of a material, and has recently been shown to closely approach the effective work function for a complete gate stack.[22] Based upon the encouraging results obtained for Si/SiO_2,[24,33] Si/HfO_2[34] and SiO_2/HfO_2[22] interfaces, we used a G_0W_0 correction hoping to provide results sufficiently close to experiment.

The G_0W_0 calculation is a perturbational approach which is generally used to correct the energy levels coming from a DFT calculation.[35] Unfortunately, one can not perform such a correction directly with SIESTA. A supplemental approximation has to be done: we performed the G_0W_0 calculations on bulk m-HfO_2 and β-SiO_2 using the plane-wave *ab initio* code ABINIT.[36] By employing Troullier-Martins-type,[27] GGA-PBE[25] pseudopotentials for ABINIT of the same nature as the pseudopotentials used with SIESTA, we were able to verify that the electronic band structures obtained in DFT with the two programs for the two bulk structures were in very good agreement. By applying a rigid shift, the band edges zones were superimposed with small differences below a few tenths of electron volt, showing that both programs were effectively solving very similar Hamiltonians with different numerical approaches. The agreement of the electronic band structure between the two *ab initio* codes allows us to apply the ABINIT many-body corrections directly to the electronic levels obtained with SIESTA as the principal effect representative of a many-body correction. A similar procedure was already employed with success for the Si/SiO_2 interface.[33]

The G_0W_0 calculations for both materials were convergence tested for the energy cutoffs, k-point grids, and number of bands in order to obtain a numerical accuracy of ± 0.1 eV for these corrections. For β-SiO_2, the density functional calculations used as the basis for the G_0W_0 used a Monkhorst-Pack[30] k-point scheme of $3 \times 3 \times 3$ without a shift to include the Γ point in the G_0W_0 calculations and an energy cutoff of 50 Ha for the wave functions. Then for the G_0W_0 calculation, we used 500 energy bands, a cutoff of 15 Ha for the dielectric matrix for the independent-particle susceptibility calculation, 20 Ha for the wave functions and 25 Ha for the self-energy operator. The DFT basis calculation for m-HfO_2 used a Monkhorst-Pack k-point sampling of $3 \times 3 \times 3$ and an energy cutoff of 80 Ha. The G_0W_0 parameters for HfO_2 used 700 energy bands, an energy cutoff of 16 Ha for the wave functions for the dielectric matrix, and energy cutoffs of 27 and 30 Ha for the wave functions and the self-energy operator respectively. Finally, the plasmon pole model proposed by Godby[37] was used to construct dielectric function for use in the G_0W_0 approximation.[34]

C. VBO at interface

The VBO between HfO_2 and SiO_2 is obtained with a two step method.[32] Firstly, we extract the macroscopic electrostatic potential as a function of the distance perpendicular to the interface. Secondly, by assuming that both materials reach their bulk states sufficiently far away from the interface, we use the energy differences between the bulk electrostatic potential and the valence band of each material to evaluate the VBO as explained below. For comparison, the obtained result can be checked using the partial density of states of each bulk region of the material (see Sec. IV A).

To determine the macroscopic electrostatic potential of the interface, we take the Kohn-Sham potential minus the exchange-correlation potential and sum up the potential in the plane parallel to the interface. This produces a unidimensional electrostatic potential in the direction perpendicular to the interface, $\overline{V}(z)$, that oscillates with as many periods as atomic planes within each material.[38,39] This microscopic electrostatic potential is then filtered through a generalized convolution for

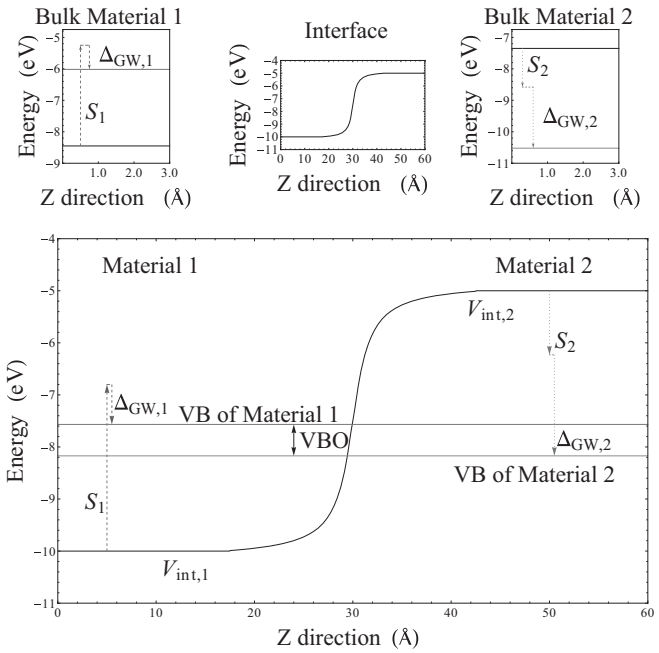

FIG. 1. The insets above show the three components, the energy difference between the valence band and the electrostatic potential for each bulk material, the G_0W_0 correction to the valence band energy, and the electrostatic potential for the interface, combined in the main image to determine the valence band offset (VBO) of an interface.

different lengths, l_i, that represent the spacings between atomic planes for both materials (four filtering lengths were needed for the HfO_2/SiO_2 case) yielding the macroscopic potential $\overline{\overline{V}}$. This filtering technique eventually produces two plateaus that correlate to the bulk properties of HfO_2 and SiO_2. The electrostatic potential is related to the macroscopic dipole through Poisson's equation.[38]

The next two quantities that are required are the energy differences between the bulk electrostatic potential and the valence band for HfO_2 and SiO_2. First, the macroscopic electrostatic potential is determined, as above, for the bulk materials. The energy difference between the constant potential and the valence band is then easily determined. However, this produces an energy difference that suffers from the band gap problem in DFT where the exact energy of the bands is offset from its correct positions.[33] A G_0W_0 calculation is performed to correct the energy difference for each material.

This procedure is illustrated in Fig. 1. The relations between these calculated values can be described by

$$E_{v,i,\mathrm{int}} = V_{\mathrm{int},i} + (S_i + \Delta_{\mathrm{GW},i}) \tag{1}$$

$$\mathrm{VBO}_{\mathrm{int}} = E_{v,\mathrm{HfO_2,int}} - E_{v,\mathrm{SiO_2,int}} \tag{2}$$

$$\mathrm{VBO}_{\mathrm{int}} = (S_{\mathrm{HfO_2}} + \Delta_{\mathrm{GW,HfO_2}}) - (S_{\mathrm{SiO_2}} + \Delta_{\mathrm{GW,SiO_2}}) + \Delta V. \tag{3}$$

Here $V_{\mathrm{int},i}$ is the value of the electrostatic potential of material i in interface int, S_i is the energy difference between the valence band and the electrostatic potential for bulk material i obtained in DFT, $\Delta_{\mathrm{GW},i}$ is the G_0W_0 correction to the valence band energy, $E_{v,i,\mathrm{int}}$ is the energy of the valence band, $\mathrm{VBO}_{\mathrm{int}}$ is defined as the valence band offset, and ΔV is the potential step that can be approximated to first order by a dipole localized at the interface defined by a charge density, σ, and spacing at the interface, d, related by

$$\Delta V = 4\pi\sigma d. \tag{4}$$

D. Density of states

Based on the DFT calculation of the interface, the density of states (DOS) is calculated with a peak broadening parameter of 0.2 eV and has 750 data points in a range of 40 eV. As SIESTA[26] uses atomic orbitals, an approximation to the partial density of states (PDOS) for specific ions or orbitals, exists. While this decoupling of states to get the PDOS is a numerical artifact, it still allows for an insight into the contributions of specific ions for gap states or to check the VBO by projecting the electronic states onto the two "bulk" regions of HfO_2 and SiO_2. This provides an alternative method to evaluate the VBO within DFT in direct comparison to the previous macroscopic averaging technique before applying the many body corrections. Because the PDOS method directly includes the effects of any deformation or stress inside the bulk regions, it permits the investigation of the error made with the macroscopic averaging technique due to the hypothesis of recovering of a fully relaxed bulk structure sufficiently far away from the interface.

III. SYSTEM CONSTRUCTION

A. Interfaces

The precise structures at the atomic scale of the HfO_2/SiO_2 interfaces that exist in CMOS devices are largely unknown. The construction of a such an interface has to be based on what is experimentally characterized, while being constrained to remain compatible with the use of *ab initio* methods and tools on current computing technology. Of particular interest in this paper are the proper choice of the phases of the two materials, the surface plane directions that were used in the interface and the nature of chemical bonds between materials. The parameters and comparisons which created and validated the interface are pivotal for any discussion.

In CMOS devices and experimental Si/SiO_2 interfaces, SiO_2 is seen to be globally amorphous.[40–42] However, studying amorphous systems using *ab initio* techniques can be quite computationally expensive due to the number of atoms involved. High resolution transmission electron microscope (HRTEM) images reveal that at the interface between Si and SiO_2 a crystalline layer consistent with the Si structure exists,[42] which has been identified as a cristobalite phase in SiO_2.[40,41] Computationally, using classical molecular dynamics simulations with *ab initio* derived interatomic potentials, Fischer *et al.* have also seen a stable pseudocristobalite phase.[43] Therefore the phase of SiO_2 used for the construction of the interfaces in this paper is β-cristobalite SiO_2, consistent with previous *ab initio* calculations.[8,13,21,44] Note that a secondary reason for using β-cristobalite is the similar density between amorphous SiO_2 grown on a Si substrate and β-cristobalite:[45] 2.20 g/cm^3 versus 2.33 g/cm^3.

Likewise, the HfO_2 phase that is seen in CMOS devices is also amorphous for the thin films of thickness <3–8 nm.[46,47]

However, for larger thicknesses, it has been seen experimentally that HfO_2 crystallizes into a monoclinic phase.[48] Due to the thermal budget during film deposition, with temperatures below ∼450 °C, the HfO_2 films are more likely to be amorphous for films <5–8 nm,[46] but Cho *et al*. showed that annealing 6.5-nm films produces a crystalline phase[47] and Kwon *et al*. show that TaN capped and no metal capped HfO_2 gate stacks crystallize into a monoclinic-phase at 500 °C.[49] This implies that the amorphous structure is approaching the monoclinic phase with a small thermal barrier between the two phases. Therefore, the monoclinic phase of HfO_2 is used here.

Following the choice of the phases of the two materials, several energetically favorable surfaces were constructed for each material. This process started with a geometry optimization of both of the bulk phases. For HfO_2, the results of the geometry optimization yield atomic positions and unit cell structure comparable with the experimental and computational values found in the literature, as shown in Appendix. Following the determination of the bulk unit cell, the four surfaces predicted to be the most favorable by Mukhopadhyay *et al*.[50] were constructed to be O terminated. Mukhopadhyay predicts that the $(\bar{1}11)$, (111), and $(\bar{1}01)$ surfaces are energetically favorable while the final surface, (001), is kinetically favorable. The surface energy per surface area, ΔG_f^{surf} is defined as

$$\Delta G_f^{\text{surf}} = \frac{E_{\text{sys}} - n\,\mu_{\text{bulk}} - p\,\frac{\mu_{O_2}}{2}}{2\,A}. \tag{5}$$

Here, E_{sys} is the internal energy of the surface system, μ_{bulk} is the chemical potential of a single bulk periodic cell, μ_{O_2} is the chemical potential of an isolated O_2 molecule, n is the number of unit cells used to construct the surface system, and p is the number of oxygen atoms used to symmetrically O terminate the surfaces. Using Eq. (5), the surface energies we found predict a stability ordering of $(\bar{1}11) > (111) > (\bar{1}01) > (001)$, which matches the result of Mukhopadhyay within a 0.2 eV/Å^2 of computational error as shown in Table I.

The surfaces of SiO_2 were constructed in a similar manner. The bulk structure was geometry optimized and shown to match the accepted values of literature[51] as seen in Appendix. The (111), $(\bar{1}11)$, (101), and (−110) surfaces were those constructed for the β-cristobalite SiO_2 because they are the highest symmetry directions in SiO_2.

Constructing a representable interface from two materials with a collection of favorable surfaces requires balancing the strain involved in adjoining the two surfaces, where two principle sources of strain can be identified. The first source is the strain generated by placing two materials of different lattice constants together. The SiO_2 unit cell parameters were used as the unstrained material with the HfO_2 strained to the SiO_2 parameters, because during the growth process, the HfO_2 is deposited onto the SiO_2. During the construction of the interfaces, we select a maximum allowable mismatch of ∼5% between the unit cell vectors and a mismatch of 5° in the angle between the vectors. These limits are still large from a macroscopic point of view. The oxide would not be expected to remain crystalline in its monoclinic state of lower energy under such strain with a Young's modulus of 220 GPa[52] for HfO_2, which is consistent with the amorphous nature of HfO_2.[46,47]

TABLE I. The surface energies of the HfO_2 $(\bar{1}11)$, (111), $(\bar{1}01)$, and (001) surfaces.

	Surface energies (J/m^2)			
	$(\bar{1}11)$	(111)	$(\bar{1}01)$	(001)
Present work	1.21	1.44	1.53	1.65
Mukhopadhyay[a]	0.99	1.20	1.32	1.42

[a]Reference 50.

The second source of interfacial strain comes from aligning the bonds in between the surface atoms of the two materials. Since monoclinic HfO_2 and β-cristobalite SiO_2 do not share the same crystal structure, the bond alignment between atoms at the interface is expected to be very different from the bulk structures which can create a large strain in individual atoms at the interface. To minimize this effect, we follow what is done experimentally: the SiO_2 is grown first, leaving a reactive O-terminated surface. We then placed the HfO_2 structure such that the oxygen atoms from the SiO_2 is located near the oxygen sites of HfO_2, which is effectively the electron counting method.[53] In practice, the O's at the interface, can be under-coordinated, but they are kept sufficiently coordinated to prevent gap states, as shown in the DOS in Sec. IV. Effectively, this means that the oxygen sites between the HfO_2 and the SiO_2 are aligned when geometry optimized, by forming Hf-O-Si bridges. This typical structure seems to be an essential characteristic of our models as shown later. Nevertheless, depending on the initial strain of the interface atoms even with a low unit cell strain some of our larger systems would not converge, which demonstrates that this chemical bonding strain for these systems was unphysical.

Coupled with the two strain reduction criteria, two computational constraints were employed. The first was the size of the supercells, which were constrained to be below 100 atoms for computational efficiency reasons. Secondly, the systems were constructed such that the periodic boundary conditions lead to two almost symmetrical interfaces to prevent the creation of an artificial potential field along the supercell.[54] Note that we also relax the stress along the stack direction.

Following this set of rules, this method yields two systems, the monoclinic HfO_2 (001)/β-cristobalite SiO_2 (101) interface (orientation A) with an in-plane tensile strain of 3.5% for the (100) direction and 2.6% for the (010) direction in the HfO_2 and the monoclinic HfO_2 (-101)/β-cristobalite SiO_2 (−110) interface (orientation B) with an in-plane tensile strain of 2.6% for the (010) direction and 7.7% for the (110) direction in the HfO_2. These interfaces are shown in Fig. 2 with the atomic and cell structures given in Supplemental Material.[55] It is worth noting that while the crystal structures of the A orientation remain consistent throughout the HfO_2 in the B orientation shows a deviation from the monoclinic phase at the interface.

In order to see how the interfaces are energetically favorable, we defined the formation energy per unit area ΔG_f as

$$\Delta G_f = \frac{E_{\text{sys}} - n\,\mu_{HfO_2} - m\,\mu_{SiO_2} - p\,\frac{\mu_{O_2}}{2} - q\,\mu_{\text{dop}}}{2\,A}. \tag{6}$$

Here, E_{sys} is the total energy of the system, μ_{HfO_2}, μ_{SiO_2}, and μ_{O_2} are the chemical potentials of bulk HfO_2, bulk SiO_2, and an oxygen molecule, μ_{dop} is the chemical potential

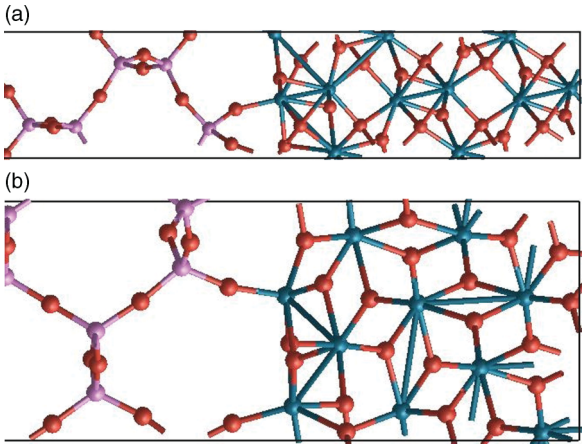

FIG. 2. (Color online) (a) The monoclinic $HfO_2(001)/\beta$-cristobalite $SiO_2(101)$ interface, labeled as the A interface. (b) The monoclinic $HfO_2(\bar{1}01)/\beta$-cristobalite $SiO_2(\bar{1}10)$ interface, labeled as the B interface. The atoms are designated as blue for Hf, red for O, and purple for Si.

of a single dopant obtained from a common phase, and n, m, p, and q are the integer values of the amount of each species present. For these reference interfaces, $\mu_{\text{dop}} = 0$. The formation energies for each interface are shown in Table II. It is important to note that the positive formation energy is a sign that the interface is less stable than the corresponding collection of components in their infinite reservoirs. This is reasonable within the assumption that an entropy of mixing term, which arises with chemical mixing of the constituents, can be neglected in these sharp interfaces. Knowing that the system of reference for oxygen is the O_2 gaseous species, we see that the chemical potential of oxygen is the variable most influential upon the interface energy, and that our models A and B can be considered oxygen rich.

B. Inclusion of dopants

We can use our reference systems to study dopant inclusion by incorporating Al, Mg, and La in substitution for individual cations. These metals are expected to either exist within the structure of the HfO_2 or SiO_2 or to strain the system to match their native oxide. Therefore all the metals are studied in each Si and Hf site within one crystalline layer of the interface with an optimization of atomic positions only followed by a VBO calculation.

Following the substitution, it is important to consider the nature of the chemical bonding of the metal dopants with the interfaces. Specifically, it is the stoichiometry of the dopant incorporation that must be consider. Sharia *et al*. studied the stoichiometric effects of an Al monolayer at the interface between HfO_2 and SiO_2.[8] If the metal dopants are incorporated during the chemical vapor deposition used for the creation of the interface, it is reasonable to assume a chemical rational such as stoichiometry to determine the dominant structure of the dopant. However, when the dopants diffuse from a capping layer to the HfO_2/SiO_2 interface, purely chemical reasoning can no longer be used to determine the structure of dopants. This is strongly supported by Bosman *et al*., who show a distribution of dopant locations for La_2O_3 and Al_2O_3 capping layers ranging from the capping layer through the HfO_2 and SiO_2 layers.[7] Therefore, to consider the complete variety of the variability issue, both the cases of stoichiometric and nomstoichiometric systems must be considered. Here, the nomstoichiometric case is considered.

When a column 4 element like Si or Hf is substituted by a column 2 or 3 element within DFT, one of two things must occur. The first is to explicitly consider the nomstoichiometry and to explicitly treat the system as a charged system by removing electrons. The other method is for a hole state to be generated in proximity to the nomstoichiometric defect. Since here we are concerned with a nomcharged interface, we let DFT determine the hole states. It is important to note that it has been shown that often DFT doesn't appropriately localize the hole unless the hole is strongly localized.[56] However, for each of the dopants we saw that the holes were localized.

TABLE II. The formation energy per unit area for the dopant free interface. The reservoirs used are the bulk forms of the HfO_2 and SiO_2.

	Interface	ΔG_f (J/m^2)
(A)	HfO_2 (001)/SiO_2 (101)	2.52
(B)	HfO_2 ($\bar{1}$01)/SiO_2 ($\bar{1}$10)	2.45

IV. RESULTS AND ANALYSIS

A. Valence band offset

1. Bulk calculations

For SiO_2 the many body G_0W_0 calculation predicts a valence band shift Δ_{GW,SiO_2} of -1.9 eV, with a corresponding band gap of 8.3 eV, as shown in Table III. The calculated band gap is in relative agreement with the accepted literature value determined by tight-binding calculations and experiment of 8.9 eV for amorphous SiO_2.[57,58] Our G_0W_0 calculations for HfO_2 predict an indirect band gap of 5.9 eV, with a valence band shift Δ_{GW,HfO_2} of -0.8 eV. This band gap is in reasonable agreement with experimental results of 5.82 eV (see Ref. 59) for a HfO_2 thin film on SiO_2. Also, Cheynet *et al*. found the band gap to be 5.9 ± 0.5 and 5.25 ± 0.5 eV for poly-Si and poly-Ge capped HfO_2 gate stacks.[60]

By running a DFT calculation for the valence band of the material and using the macroscopic electrostatic potential, the difference (S_{SiO_2}) is calculated to be -1.6 eV for SiO_2, while the difference (S_{HfO_2}) is $+3.3$ eV for HfO_2.

2. Reference interfaces

Looking at the macroscopic potential for each reference interface, A and B, shown in Fig. 3, the regions approaching bulk properties of each material are characterized by

TABLE III. The $\Delta_{GW,i}$, S_i, and E_{Gap} for HfO_2 and SiO_2. The experimental band gap for SiO_2 was for an amorphous system.

	$\Delta_{GW,i}$ (eV)	S_i (eV)	E_{Gap} (eV)	Exp. E_{Gap} (eV)
SiO_2	-1.9	-1.6	8.3	References 57 and 58
HfO_2	-0.8	$+3.3$	5.9	Reference 59

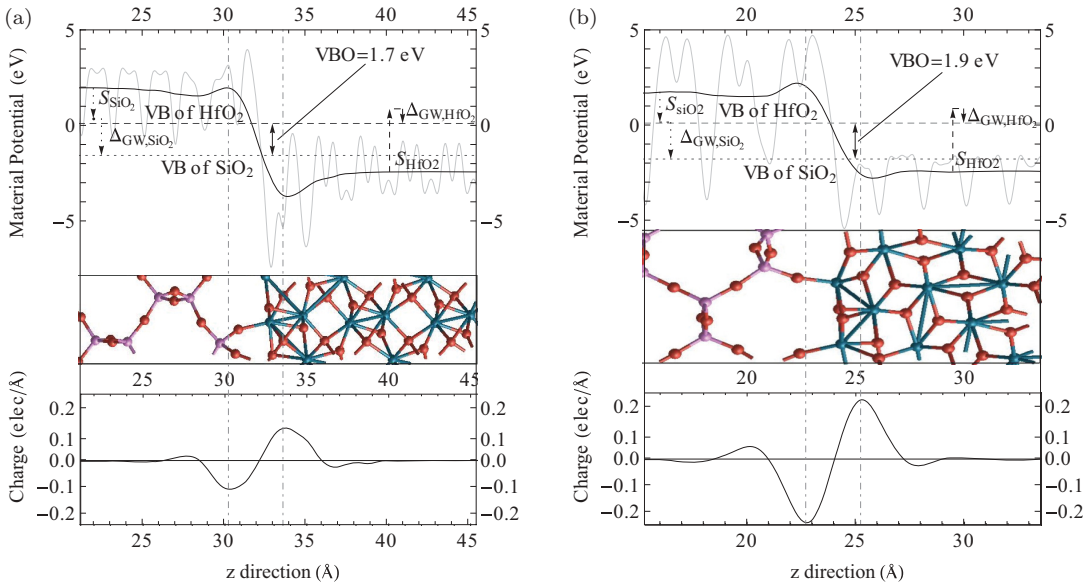

FIG. 3. (Color online) Plots of the electrostatic potential, the atomic structure, and the total charge density for the (a) $HfO_2(001)/SiO_2(101)$ (labeled the A interface in the text), and (b) $HfO_2(\bar{1}01)/SiO_2(\bar{1}10)$ (labeled the B interface in the text) interfaces, aligned along the z direction. In the electrostatic potential plots, the black curve is the macroscopic potential and the gray curve is the microscopic electrostatic potential. The energy zero is set to be the VB of HfO_2 since this corresponds to the Fermi energy of the system. The vertical dashed lines show the location of the primary dipole peaks. The atoms are designated as blue for Hf, red for O, and purple for Si.

approximately flat regions of the macroscopic electrostatic potential as expected, which determines $V_{\text{int},i}$. Substituting $V_{\text{int},i}$ for each of the two materials into Eqs. (1) and (2) for each of the two reference interfaces yields a G_0W_0 corrected VBO_A of 1.7 eV and a (G_0W_0) corrected VBO_B of 1.9 eV. These two G_0W_0 corrected results agree well with the range seen from XPS measurements, which give a VBO of 1.0–1.9 eV[61,62] (note that without the additional G_0W_0 correction the VBO for interface A is 0.5 eV and 0.7 eV for interface B). Our VBOs vary slightly from electrical measurements of Charbonnier *et al.*, which have a VBO of about 2.1 eV.[63] This difference can be attributed to *N* diffusion and different thermal budgets in the experiment, or to our selection of specific variations for the interfaces. This agreement is necessary, but not sufficient in demonstrating the validity of our models as a basis for pursuing the analysis of the induced dipoles and VBO shifts caused by the inclusion of dopants. However, when this is combined with the reduction of forces on the interfacial atoms due to the bridging oxygen, the reduced interfacial strain (for an expected amorphous systems), and the lack of interface induced gap states, as described below, these reference systems are expected to be appropriately predictive.

To further confirm the accuracy of the electrostatic potential method, the PDOS calculated by SIESTA[26] was used. The valence bands (VBs), determined by this method should in principle give the same VBO as the electrostatic potential method without G_0W_0 correction. However, when the VBs are determined by each method are compared for both orientations a difference of ±0.2 eV is seen. This is specifically due to the approximation that the HfO_2 and the SiO_2 return to their bulk properties far from the interfaces. Based upon the way the interface systems were constructed, we know that the HfO_2 is constrained to the unit cell of the SiO_2. This constraint prevents the HfO_2 from being in its minimum energy configuration. Based on the same finding, Sharia *et al.* found a difference of between ±0.1 and ±0.2 eV for cubic and monoclinic HfO_2 systems.[21]

As is known in classical electrodynamics, the source of a potential difference is the existence of a macroscopic dipole at an interface. By extracting the total average charge density from the three-dimensional total charge density, using the same averaging and filtering techniques used to generate the average electrostatic potential as a function of *z*, we are able to directly relate each VBO to its macroscopic dipole, as illustrated in Fig. 3. These dipoles arise because the valence electron density for HfO_2 (0.45 $e^-/\text{Å}^3$) is significantly larger than that of SiO_2 (0.29 $e^-/\text{Å}^3$), as shown in Table IV. Therefore, when the two materials are put together at an interface, an imbalance is created that results in a charge build up at the interface. A negative charge is expected to build up outside the high electron material (HfO_2) as the increased valence electron density trails off to the decreased value of the SiO_2 like a metal with a vacuum surface. From Fig. 3, we see that the majority of the negative charge accumulate on the first SiO_2 plane and the interfacial O, which plays a key role in bridging between the two materials. This results in a positive charge build up at the last HfO_2 plane

TABLE IV. The average valence electron density, $\bar{\rho}_{\text{val}}$, and average *X*-O bond length, $l_{X\text{-O}}$(Å), determined by DFT calculation for the bulk oxide cell.

Oxide	$\bar{\rho}_{\text{val}}$ ($e^-/\text{Å}^3$)	$l_{X\text{-O}}$ (Å)
Al_2O_3	0.55	1.9
HfO_2	0.45	2.1
MgO	0.42	2.1
SiO_2	0.29	1.6
La_2O_3	0.28	2.6

due mainly to a lower coordination number for the hafnium atoms at the interface. This build up of charge at the interface induces screening that generates secondary and tertiary dipoles around the primary dipole since SiO_2 and HfO_2 are insulators.

Determining the surface charge density σ_{int} by integrating dipole peaks for each of the orientations yields $\sigma_A = 0.0146\,\text{elec}/\text{Å}^2$ for the A orientation and $\sigma_B = 0.0144\,\text{elec}/\text{Å}^2$ for the B orientation. This small difference between σ_A and σ_B cannot explain the difference in the VBO between the two systems. However, if we then refer to Eq. (4), we can estimate ΔV by multiplying σ by $4\pi d$, where d is the distance between the major dipole peaks. This distance is 3.4 Å in system A and 2.6 Å in system B. Using these values gives a difference of ~2 eV between the two systems, which overestimates the difference by an order of magnitude. However, this equation considers the charge as a point in a 1D electrostatic problem. Therefore we see that the shape at the atomic scale of the dipole greatly modifies the potential step between the two materials. Using the 1D solution to the Poisson equation,

$$\overline{\overline{V}} = -2\pi \int_{-\infty}^{\infty} \overline{\overline{\rho}}(z')|z - z'|dz', \tag{7}$$

we confirm that the macroscopic total charge density, $\overline{\overline{\rho}}(z)$, calculated by DFT generates exactly the same potential, $\overline{\overline{V}}$, as the DFT calculation. This demonstrates the importance of the microscopic charge structure (the curve shape) to the VBO.

3. *Doped systems*

Now, we consider the effect of single cation substitution, of La, Al, or Mg, for Hf or Si at the first atomic plane of the interface, upon the VBO. Figures 4(b) and 5(b) plot the VBO versus the energy of formation of the respective interfaces for each dopant location. The energy of formation of different types of defects is strongly dependent upon each constituent material used for the chemical potentials μ_{dop}, as demonstrated in Eq. (6). The constituents used are γ Al_2O_3 for Al, halite cubic MgO for Mg, and hexagonal La_2O_3 for La. In reality, the choice of constituents is dependent upon the exact growth process and the different thermal treatments. For example, O can be provided by many materials during the growth process, including but not limited to O_2, H_2O, and hydrocarbons. Also, this choice of constituents depends upon the method of the defects creation. If the defect diffuses through the interface during thermal treatments, it is also possible to use silicates for the chemical potentials. However, this is not done here because we are treating the defects as single substitutions at a sharp interface. Another consideration is that the stoichiometry of the interface also affects whether a bulk metal should be used instead of its oxide. Therefore the formation energy should only be used as a qualitative measurement of stability in these plots instead of as a definitive energy ordering of specific defects.

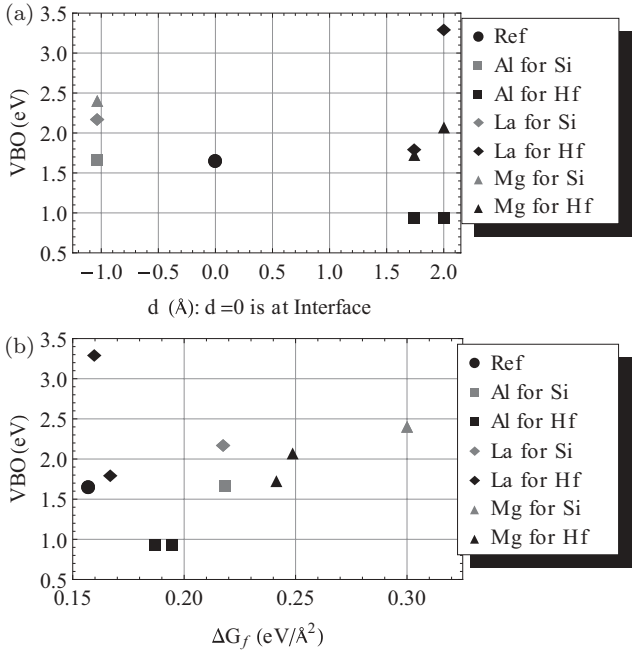

FIG. 4. A plot of the VBO for different defects in the $HfO_2(001)/SiO_2(101)$ interface system (a) vs distance from the interface, d, and (b) vs formation energy. The reference system, Ref, is the dopant free interface.

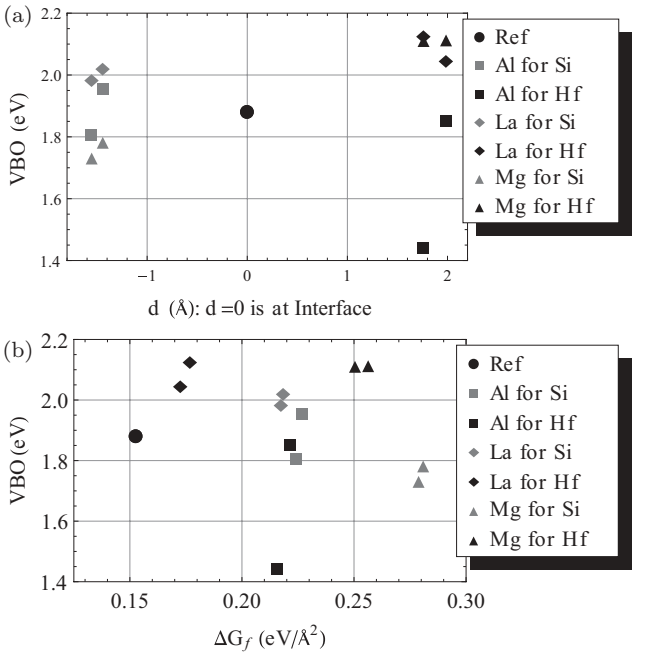

FIG. 5. A plot of the VBO for different defects in the $HfO_2(\bar{1}01)/SiO_2(\bar{1}10)$ interface system (a) vs distance from the interface, d, and (b) vs formation energy. The reference system, Ref, is the dopant free interface.

As it appears in Figs. 4(b) and 5(b), the lower formation energies that are close to the reference systems are always obtained for all the dopants substituted within the HfO_2. We presume this is because the substitutions within SiO_2 would require a relaxation process that would allow the formation of silicates of the dopants. To perform such a relaxation process would require larger systems as well as an inclusion of a thermal aspect that is beyond the conjugate gradient optimization we used. For specific substitutions, particularly for the lower formation energy substitutions within the HfO_2, we reproduce the experimental expectations that La

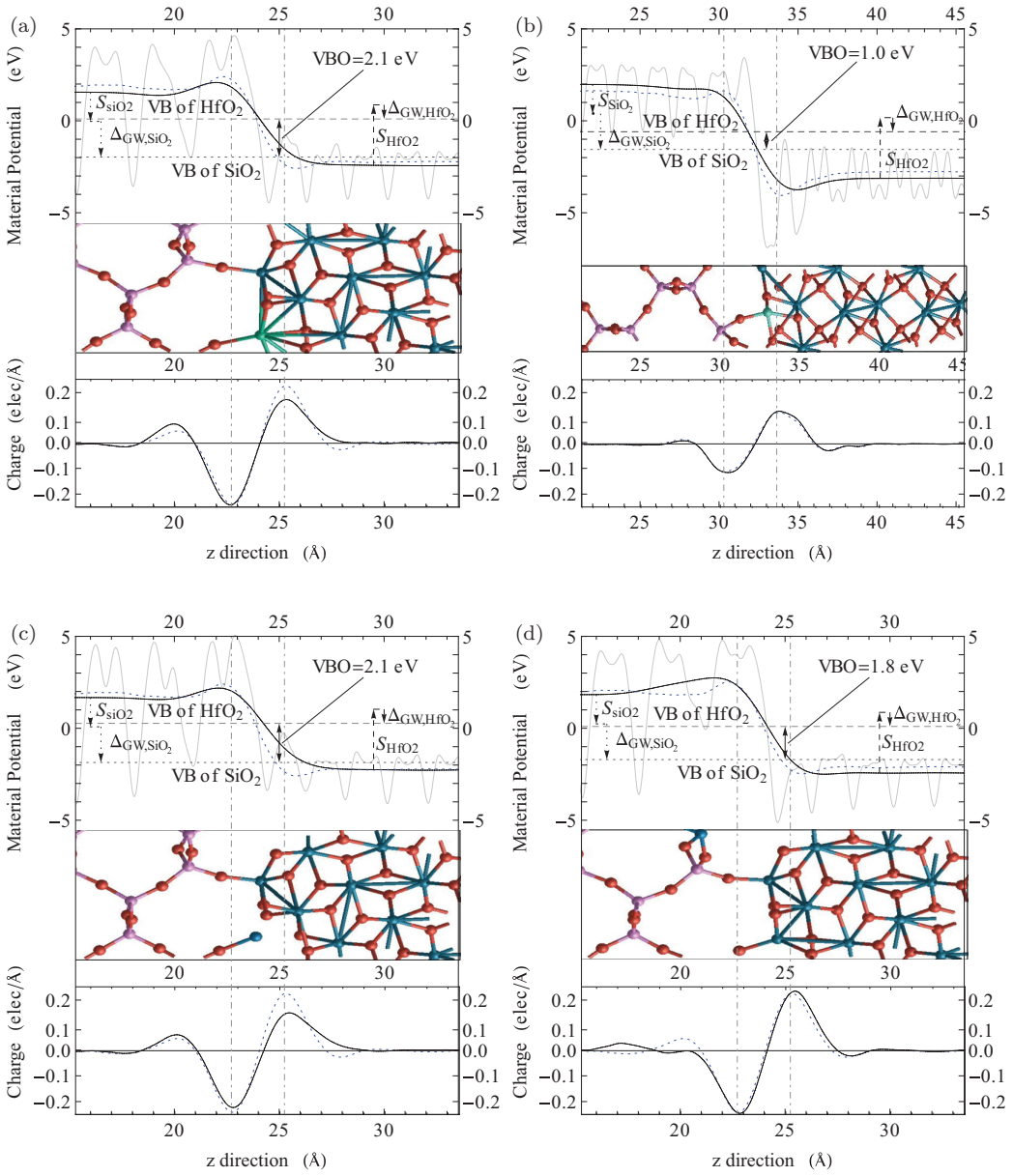

FIG. 6. (Color online) Plots of the electrostatic potential, the atomic structure, and the total charge density for the (a) La substituted for Hf in the B orientation, (b) Al substituted for Hf in the A orientation (c) Mg substituted for Hf in the B orientation, and (d) Mg substituted for Si in the B orientation. For all plots, the blue dotted curve is the respective reference system. In the electrostatic potential plots, the black curve is the macroscopic potential and the gray curve is the microscopic electrostatic potential. The energy zero is set to be the VB of HfO_2 since this corresponds to the Fermi energy of the system. The vertical dashed lines show the location of the primary dipole peaks. The atoms are designated as blue for Hf, red for O, purple for Si, teal for La, light blue for Al, and dark blue for Mg.

substitutions increase the VBO,[11] the Al decreases the VBO,[11] and Mg also increases the VBO.[64] For less energetically favorable substitutions, for example the Mg substitution of Si for system B, the resulting VBO does not follow the experimentally seen result.

We turn to the analysis of specific examples of the dipole modulation at the microscopic level due to cation dopants. The first case is La substitution for Hf in system B, which is consistent with the experimental increase of the VBO and is energetically favorable for substitution in HfO_2. The total charge density for the La dipole in Fig. 6(a) shows that the charge density for the primary dipole peak in the HfO_2 decreases consistently with the decrease in the average valence electron density of the La_2O_3, as shown in Table IV. Also, a large increase in the secondary dipole peak in SiO_2 is seen, due to the compression of the SiO_2 from the increased La-O bond length that is also shown in Table IV. To first order, it is these two changes in dipoles that create the change in the VBO due to La introduction.

The second example of a dopant system is the Al substitution for Hf in the A orientation. For this system, the primary dipole peak in HfO_2 is slightly increased due to the increase in the average valence electron density, while the increase in the primary dipole peak in the SiO_2 is due to the pulling of the SiO_2

layer by the Al-O bond being shorter than the corresponding Hf-O bond, which is then compensated by a slight decrease in the secondary dipole peak in the SiO_2.

For the Mg substitution for Hf in the B orientation, the fact that Mg tends to recover its rock salt structure by producing a stretched O-Mg-O bond at the interface generates a highly nonsymmetric dipole with the secondary dipole responding to preserve the neutral electronic polarization of the system. This coupled with the slight decrease in the average valence electron density between MgO and HfO_2 results in a increase in the VBO, showing also a strong similarity with the La case.

The Mg substitution for Si in the B orientation is analyzed as an exceptional case, because it is not in agreement with the (few) experimental values obtained for Mg and also because of its high energy of formation. The incorporation of Mg inside SiO_2 causes the disappearance of the secondary peak of charge depletion for the secondary dipole inside SiO_2, which is probably simply due to the reduced number of valence electrons that Mg can provide compared to Si. This tends to increase the primary peak close to the bridging oxygen that is compensated by the increase of the primary peak at the HfO_2 side, resulting in a global increase of the dipole that corresponds to a VBO decrease for Mg, contrary to the preceding substitution.

To globally explain the variation of the change in the VBO with dopant inclusion, a comparison between average valence electron density of the dopant's oxide and of the material of substitution is used, along with a study of the X-O bond within the dopant's oxide, as seen in Table IV. If the electron density of the dopant's oxide is larger than the average valence electron density of the substituted oxide, then the VBO can shift downward due to an increase of electrons in the surface dipole, while a smaller density results in an increase in the VBO due to the reduced dipole at the interface. Therefore this predicts that Al will always show a tendency for a negative ΔVBO, La a tendency for a positive ΔVBO, while Mg will be positive for substitutions in the HfO_2 and negative for the SiO_2. Modulations and even deviations in these trends can be described due to the difference in the X-O bond length as shown in the specific examples described above. In some cases, it is felt that large re-arrangements modify the structure of the interface in such a way that the predictions based upon the average valence electron density can become a less dominant effect. Also, the change in orientation of the interface is expected to modulate the electron density immediately at the interface and therefore modify this model.

To conclude, studies of the response of the bonding structure and charge density profiles show that small changes in the shape of interfacial dipole strongly affect the electrostatic potential, and hence the VBO. In addition, the dipole extends several layers into each material with the low magnitude tails of the dipole playing a significant role. Finally, the size of the dipole with respect to defect type and the corresponding change in VBO requires a DFT calculation to capture the complexity of the system as shown by the charge as a function of the z direction in Fig. 6 where several peaks are identifiable. Specifically, it is the primary peak and trough that determine the magnitude of the large step between the potentials of the two materials with the secondary peaks providing the size of the trough or horn that determines the final modulation of the electrostatic potentials before they reach the "bulk" regions of the materials.

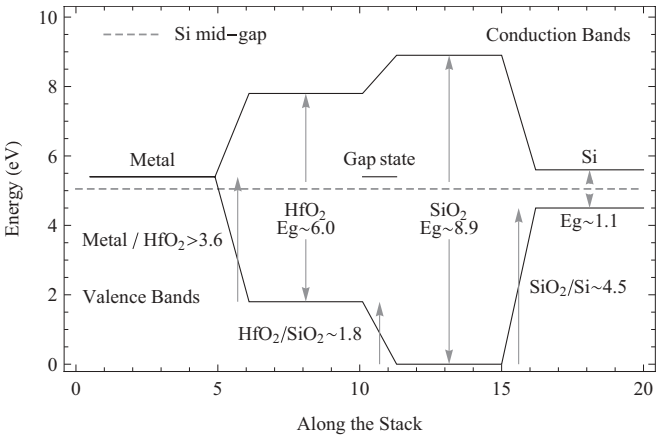

FIG. 7. A plot of the valence and conduction bands of a typical HfO_2/SiO_2 gate stack with a gap state included at the HfO_2/SiO_2 interface. Note that the gap state is close to the metallic Fermi energy and Si mid gap, creating the possibility of a tunneling current.

B. Density of states

Of particular importance is to know if defects at the interface induce the existence of electronic states within the band gap, which in principle could generate a charged system when a given voltage is placed across the interface, but also facilitate any tunneling leakage current assisted by traps. For example, Sharia *et al*. discussed the creation of these gap states as a result of nomstoichiometric Al inclusions during their study of the effects of stoichiometric Al_2O_3 monolayers at the HfO_2/SiO_2 interface.[8]

Figure 7 shows the theoretical arrangement of the valence and conduction bands of a high-κ gate stack using values from the literature. A gap state is also included at the HfO_2/SiO_2 interface near the Fermi energy of the metal. The energy difference between the silicon valence band (or the metal Fermi energy) and the gap state is sufficiently small allowing electrons to tunnel from the silicon channel to the gap state and on to the metal inducing a tunneling current. Quantifying this tunneling current requires not only the exact knowledge of the band offset of the entire gate stack, but also knowledge of the dominant tunneling current pathway, the defect density of the gate stack, and the modifications of the electronic structure due to a charged state. Of course, such an understanding is beyond the scope of this paper, we cover here only the rough localization of possible gap states in energy for a neutral system, taking into account the indetermination relative to the valence and conduction bands due to the known DFT limitation.

Before a discussion of the effects of dopants, it is important to look at the density of states of the reference interfaces A and B, shown in Fig. 8 (without any G_0W_0 correction). These two DOS plots show a clean gap related to the HfO_2 oxide that is slightly diminished by the interface states when compared to the bulk system. Therefore the bridging oxygen between HfO_2 and SiO_2 and the reconstructions of both oxides do not induce localized states with an energy inside the gap.

We turn now to Al, La, and Mg, substitutions for Si and Hf atoms. The results of a methodical study of all

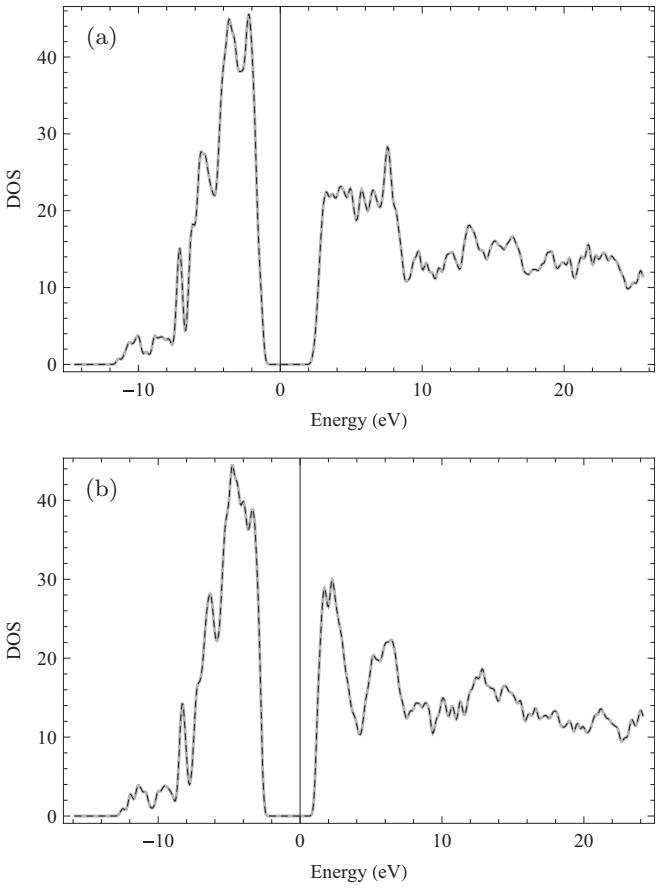

FIG. 8. The density of states of the (a) $HfO_2(001)/SiO_2(101)$ and (b) $HfO_2(-101)/SiO_2(-110)$ reference systems. The Fermi energy is defined to be zero. Both spins are represented with spin up black and dashed and spin down gray and solid.

available substitutions yields the following results, with Fig. 9 displaying an example of each result. (a) For the Al in HfO_2 or SiO_2 for both A and B orientations, an empty state appears just over the valence band, slightly more detached from the valence band for the Si substitution case. (b) For the Mg defects, an empty state was created for all locations and both orientations that ranged from a valence band shoulder state to just below mid gap. The systems that have higher gap state energy tended to be the substitutions for Hf in the A orientation. (c) La in the A orientation shows one gap state in the lower-energy range of the band gap when substituted for Hf and has two gap states in the lower portion of the band gap with one bordering the valence band when substituted for Si. (d) La in the B orientation does not have a gap state for either substitution. However, the valence band of one spin is shifted to slightly higher energy.

Since all of the dopants considered here are nomstoichiometric when substituted into HfO_2 or SiO_2 it is sensible to assume the gap states are caused due to this nonstoichiometry, which agrees with Sharia *et al.*[8,21] who, as discussed above, predicted this for the case of Al and Al_2O_3. To confirm this for Al, we used two approaches. The first was to use the orbital decomposition of the electron wave function inherent in the SIESTA[26] code to identify the source of the gap states. The defect was seen to be a state contributed by an interfacial O ion. For the second approach, we constructed a stoichiometric Al_2O_3 layer by Al substitutions for Hf and removing an O ion (several cases where run with different O ion selected) and no gap states were seen. Between the stoichiometric treatment of Al_2O_3, and determining that the source of the gap state to be the additional O atom, it is strongly suggested that the lack of stoichiometry is also the source of a majority of the gap states in the interface for La and Mg. Taking into account that a Mg substitution is the more pronounced case for nonstoichiometry (MgO versus HfO_2 or SiO_2), this could explain why peaks are more pronounced in this case.

V. CONCLUSIONS AND DISCUSSION

In an *ab initio* framework, using standard DFT tools employing a GGA functional, we derived two reference systems for the HfO_2/SiO_2 interface with two different orientations for monoclinic HfO_2 and β-cristobalite SiO_2: $HfO_2(001)/SiO_2(101)$ and $HfO_2(\bar{1}01)/SiO_2(\bar{1}10)$. These

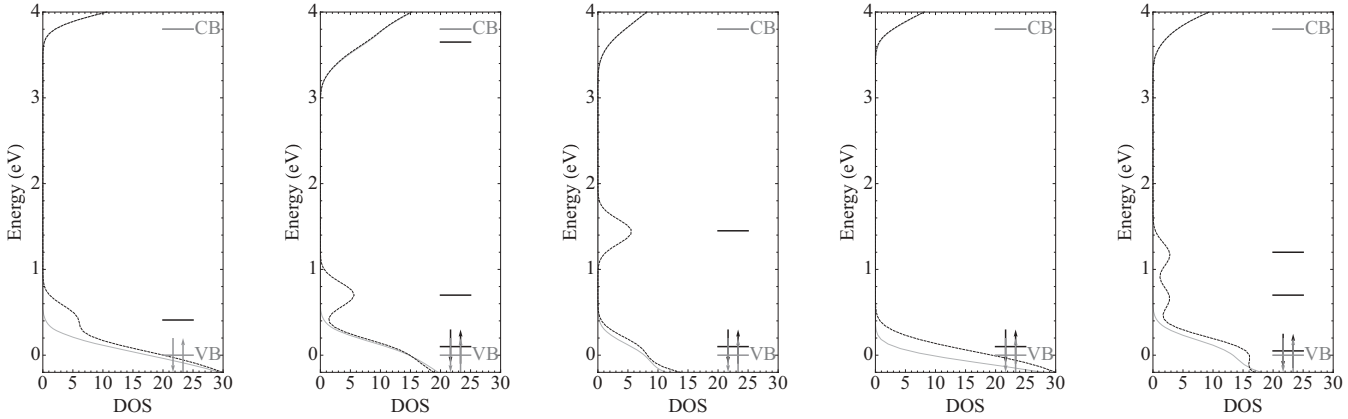

FIG. 9. The density of states of spin up (black) and spin down (gray) electrons for the metal substitution of (a) Al for Hf in the $HfO_2(001)/SiO_2(101)$ orientation (b) Al for Si in the $HfO_2(\bar{1}01)/SiO_2(\bar{1}10)$ orientation (c) Mg for Hf in the $HfO_2(001)/SiO_2(101)$ orientation and (d) La for Hf in the $HfO_2(\bar{1}01)/SiO_2(\bar{1}10)$ orientation (e) La for Si in the $HfO_2(001)/SiO_2(101)$ orientation. The valence band (VB) is set to be at 0 eV.

interfaces reveal several results that support the validity of these systems and their use for predictive studies of dopants: (a) the averaged in-plane strain imposed by the SiO_2 layer onto HfO_2 was minimized to less than $\sim$5%. (b) After minimization, both materials remain consistent to the existing experimental electrical and structural characterization results generally obtained in the CMOS technological context. (c) The bridging oxygens between the two oxides minimizes the forces on the interfacial atoms for these systems. (d) The bridging oxygen also provide electronic passivation such that the density of states is clear of gap states. (e) A realistic charge transfer is seen leading to VBOs of 1.7 and 1.9 eV that agree with XPS and electrical measurements.[61–63] (f) In terms of methodology, this good agreement with the experimental VBOs is offered by a first order G_0W_0 correction applied to the reference electrostatic potential method allowing the DFT results to be quantitatively realistic. Therefore these reference interfaces are expected to be appropriately predictive.

Nevertheless, a main source of error has been identified to be due to the stress resulting from the sticking of the two materials. Comparing the noncorrected VBOs obtained in DFT between the electrostatic potential method and the projection of the density of states along the stack axis, we obtain a difference of $\pm$0.2 eV. Looking more deeply at the atomic arrangements, we see that the large lattice mismatch leads to a complicated epitaxial relationship at the interface that prevents the two materials, especially the HfO_2 in our case, to return back to their exact bulk states. The $\pm$0.2 eV error is only a part of the story, knowing that another source of error is contained in our methodology because we didn't study the effect of strain on the G_0W_0 corrections. Finally, even the fact that only HfO_2 is constrained is objectionable, since two other sources of stress have been experimentally identified in a CMOS gate stack: (1) the stress imposed by the massive silicon substrate on the SiO_2 and (2) the stress imposed by the metal gate onto the whole stack.

This important question of VBO as a function of stress goes beyond the scope of this paper, that is focused upon dopant inclusion. The VBO as a function of stress will be the focus of a future study starting from these two reference systems (to be published by the authors).

Knowing the technological importance of diffusing metallic cations through the HfO_2/SiO_2 interface, but without knowing the precise structure of this interface nor the diffusion mechanisms involved during metal diffusion through the oxides layers, we employed our two reference systems to gauge the effect of a single dopant inclusion within the first atomic planes on either side of the interface. We extracted the ΔVBO for the dopants for each reference orientation as well as the dipole modulations due to dopant inclusion. We see that the more energetically favorable systems for each dopant represent the shifts in the VBO seen experimentally, with an increase for La and Mg, and a decrease for Al. The study of the charge dipole at the interface for these dopants reveals that comparing the average valence electron density of the bulk oxides of the dopant with the oxide it is replacing, as well as the X-O bond distance, allows for a rough description of the cause of the change in the VBO, which also supports the phenomenological analyze of Toriumi[65] up to a certain point. Despite such phenomenological analysis, it is necessary to use a self-consistent density functional calculation to capture the overall effect of a given dopant substitution. This is due to the dipole extending over 2–3 atomic layers because slight variations in the secondary dipoles leads to significant changes to the VBO. Similarly, it is important to use the 1D Poisson equation like Eq. (7) apposed to a point charge model for the interfacial charge dipole.

The second property that was studied here in relation to the included dopants of the material was the creation of gap states at the interface that could play a role in stability issues within the gate stack. All the metal dopants do generate gap states with the more pronounced effect due to Mg substituted for Hf in A orientation where a state exists near the middle of the band gap. This type of gap states could influence the gate stack system by allowing additional charge to accumulate at the interface. This would then modify the potential, driving any leakage currents as well as modifying the interfacial dipole that determines the VBO.

In conclusion, taking into account our contribution to the understanding effort of the variation of gate stacks properties due to the process steps used, we can say that examinations of additional configurations of this interface are desirable in terms of orientation, crystallinity, stress, and also other possible dopants to enrich the modeling of VBO modulation. In order to simplify this hard task, we provide the full atomic coordinates for our two reference systems in Supplemental Material for complementary studies.

ACKNOWLEDGMENTS

This work was performed using HPC resources from GENCI-CCRT (Grant 2010-096165 2011-096165). The funding for this project came from the CILOE MINALOGIC, CEA/NANOSCIENCE, and EUROTALENTS programs at the CEA.

TABLE V. The unit cell parameters and relative atomic positions of the monoclinic HfO_2 from this work (with numerical orbitals, NO, in SIESTA and plane waves, PW, in ABINIT) in comparison with literature. a, b, and c are in Å, β is in degrees, and the Hf and O locations are in fractional coordinates.

	Exp[a]	GGA[b]	GGA[c]	LDA[c]	GGA^{NO}	GGA^{PW}
a	5.117	5.079	5.291	5.106	5.175	5.137
b	5.175	5.177	5.405	5.165	5.234	5.167
c	5.220	5.250	5.366	5.281	5.341	5.336
β	99.22	99.24	97.921	99.35	99.49	99.62
Hf^1_x	0.276	0.277	0.276	0.280	0.275	0.285
Hf^1_y	0.040	0.042	0.039	0.043	0.042	0.043
Hf^1_z	0.208	0.207	0.209	0.209	0.208	0.203
O^1_x	0.074	0.075	0.089	0.076	0.072	0.076
O^1_y	0.332	0.343	0.367	0.346	0.336	0.323
O^1_z	0.347	0.336	0.317	0.337	0.341	0.348
O^2_x	0.449	0.446	0.447	0.447	0.448	0.440
O^2_y	0.758	0.759	0.759	0.759	0.759	0.756
O^2_z	0.480	0.481	0.483	0.483	0.481	0.477

[a]Reference 66.
[b]Reference 50.
[c]Reference 67.

APPENDIX

To confirm the viability of the systems used, Tables V and VI contain the bulk parameters of HfO_2 and SiO_2 compared to literature.[50,51,66,67] It is also worth noting that the crystal structure and ionic positions for the monoclinic $HfO_2(001)/\beta$-cristobalite $SiO_2(101)$ interface used in this paper are in Supplemental Material.[55]

TABLE VI. The unit cell parameter of β-cristobalite SiO_2 (with $Fd3m$ symmetry) from this work (with numerical orbitals, NO, in SIESTA and plane waves, PW, in ABINIT) in comparison with literature. Dimensions are in Å.

	GGA[a]	LDA[a]	GGA^{NO}	GGA^{PW}
a	7.417	7.352	7.591	7.444

[a]Reference 51.

[1] G. D. Wilk, R. M. Wallace, and J. M. Anthony, J. Appl. Phys. **89**, 5243 (2001).
[2] J. Robertson, Rep. Prog. Phys. **69**, 327 (2006).
[3] T. S. Jeon, J. M. White, and D. L. Kwong, Appl. Phys. Lett. **78**, 368 (2001).
[4] M. H. Hakala, A. S. Foster, J. L. Gavartin, P. Havu, M. J. Puska, and R. M. Nieminen, J. Appl. Phys. **100**, 043708 (2006).
[5] E. Gusev, C. C. Jr., M. Copel, C. D'Emic, and M. Gribelyuk, Microelectron. Eng. **69**, 145 (2003).
[6] S. Rashkeev, K. van Benthem, S. Pantelides, and S. Pennycook, Microelectron. Eng. **80**, 416 (2005).
[7] M. Bosman, Y. Zhang, C. K. Cheng, X. Li, X. Wu, K. L. Pey, C. T. Lin, Y. W. Chen, S. H. Hsu, and C. H. Hsu, Appl. Phys. Lett. **97**, 103504 (2010).
[8] O. Sharia, A. A. Demkov, G. Bersuker, and B. H. Lee, Phys. Rev. B **77**, 085326 (2008).
[9] L. Q. Zhu, N. Barrett, P. Jégou, F. Martin, C. Leroux, E. Martinez, H. Grampeix, O. Renault, and A. Chabli, J. Appl. Phys. **105**, 024102 (2009).
[10] L. Lin and J. Robertson, Appl. Phys. Lett. **95**, 012906 (2009).
[11] H. Arimura, R. Haight, S. L. Brown, A. Kellock, A. Callegari, M. Copel, H. Watanabe, V. Narayanan, and T. Ando, Appl. Phys. Lett. **96**, 132902 (2010).
[12] L. Lin and J. Robertson, J. Appl. Phys. **109**, 094502 (2011).
[13] X. Luo, G. Bersuker, and A. A. Demkov, Phys. Rev. B **84**, 195309 (2011).
[14] V. Narayanan, V. Paruchuri, E. Cartier, B. Linder, N. Bojarczuk, S. Guha, S. Brown, Y. Wang, M. Copel, and T. Chen, Microelectron. Eng. **84**, 1853 (2007).
[15] V. Paruchuri, V. Narayanan, B. Linder, S. Brown, Y. Kim, Y. Wang, P. Ronsheim, R. Jammy, and T. Chen, VLSI Technology, Systems and Applications, 2007. VLSI-TSA 2007. International Symposium (2007).
[16] G. Declerck, VLSI Technology, 2005. Digest of Technical Papers. 2005 Symposium pp. 6–10 (2005).
[17] D. Reid, C. Millar, S. Roy, and A. Asenov, IEEE Trans. Electron Devices **57**, 2801 (2010).
[18] D. Reid, C. Millar, S. Roy, and A. Asenov, IEEE Trans. Electron Devices **57**, 2808 (2010).
[19] S. Markov, S. Roy, and A. Asenov, IEEE Trans. Electron Devices **57**, 3106 (2010).
[20] A. A. Demkov, O. Sharia, X. Luo, and J. Lee, Microelectronics Reliability **47**, 686 (2007), 14th Workshop on Dielectrics in Microelectronics (WoDiM 2006).
[21] O. Sharia, A. A. Demkov, G. Bersuker, and B. H. Lee, Phys. Rev. B **75**, 035306 (2007).
[22] P. Y. Prodhomme, F. Fontaine-Vive, A. V. D. Geest, P. Blaise, and J. Even, Appl. Phys. Lett. **99**, 022101 (2011).
[23] J. Gavartin and A. Shluger, Microelectron. Eng. **84**, 2412 (2007).
[24] R. Shaltaf, G.-M. Rignanese, X. Gonze, F. Giustino, and A. Pasquarello, Phys. Rev. Lett. **100**, 186401 (2008).
[25] J. P. Perdew, K. Burke, and M. Ernzerhof, Phys. Rev. Lett. **77**, 3865 (1996).
[26] J. M. Soler, E. Artacho, J. D. Gale, A. García, J. Junquera, P. Ordejón, and D. Sánchez-Portal, J. Phys.: Condens. Matter **14**, 2745 (2002).
[27] N. Troullier and J. L. Martins, Phys. Rev. B **43**, 1993 (1991).
[28] E. Engel, A. Höck, and S. Varga, Phys. Rev. B **63**, 125121 (2001).
[29] S. G. Louie, S. Froyen, and M. L. Cohen, Phys. Rev. B **26**, 1738 (1982).
[30] H. J. Monkhorst and J. D. Pack, Phys. Rev. B **13**, 5188 (1976).
[31] S. B. Zhang, M. L. Cohen, S. G. Louie, D. Tománek, and M. S. Hybertsen, Phys. Rev. B **41**, 10058 (1990).
[32] C. G. Van de Walle and R. M. Martin, Phys. Rev. B **34**, 5621 (1986).
[33] B. R. Tuttle, Phys. Rev. B **70**, 125322 (2004).
[34] M. Grüning, R. Shaltaf, and G.-M. Rignanese, Phys. Rev. B **81**, 035330 (2010).
[35] G. Onida, L. Reining, and A. Rubio, Rev. Mod. Phys. **74**, 601 (2002).
[36] X. Gonze *et al.*, Comput. Phys. Commun. **180**, 2582 (2009).
[37] R. W. Godby and R. J. Needs, Phys. Rev. Lett. **62**, 1169 (1989).
[38] L. Colombo, R. Resta, and S. Baroni, Phys. Rev. B **44**, 5572 (1991).
[39] R. M. Martin and K. Kunc, Phys. Rev. B **24**, 2081 (1981).
[40] N. Ikarashi, K. Watanabe, and Y. Miyamoto, Phys. Rev. B **62**, 15989 (2000).
[41] N. Ikarashi, K. Watanabe, and Y. Miyamoto, J. Vac. Sci. Technol. A **21**, 495 (2003).
[42] P. Donnadieu, E. Blanquet, N. Jakse, and P. Mur, Appl. Phys. Lett. **85**, 5574 (2004).
[43] D. Fischer, A. Curioni, S. Billeter, and W. Andreoni, Appl. Phys. Lett. **88**, 012101 (2006).
[44] F. Giustino, P. Umari, and A. Pasquarello, Microelectron. Eng. **72**, 299 (2004).
[45] *CRC Handbook of Chemistry and Physics, Internet Version 2005*, edited by D. R. Lide (CRC Press, Boca Raton, FL, 2005).
[46] M. Cho, J. Park, H. B. Park, C. S. Hwang, J. Jeong, and K. S. Hyun, Appl. Phys. Lett. **81**, 334 (2002).
[47] M. Cho, H. B. Park, J. Park, S. W. Lee, C. S. Hwang, G. H. Jang, and J. Jeong, Appl. Phys. Lett. **83**, 5503 (2003).
[48] J. Niinistö, M. Putkonen, L. Niinistö, S. L. Stoll, K. Kukli, T. Sajavaara, M. Ritala, and M. Leskelä, J. Mater. Chem. **15**, 2271 (2005).
[49] J. Kwon and Y. J. Chabal, J. Appl. Phys. **107**, 123505 (2010).
[50] A. B. Mukhopadhyay, J. F. Sanz, and C. B. Musgrave, Phys. Rev. B **73**, 115330 (2006).

[51]Th Demuth, Y. Jeanvoine, J. Hafner, and J. G. Ángyán, J. Phys.: Condens. Matter **11**, 3833 (1999).
[52]K. Tapily, J. E. Jakes, D. S. Stone, P. Shrestha, D. Gu, H. Baumgart, and A. A. Elmustafa, J. Electrochem. Soc. **155**, H545 (2008).
[53]P. W. Peacock and J. Robertson, Phys. Rev. Lett. **92**, 057601 (2004).
[54]J. Goniakowski, F. Finocchi, and C. Noguera, Rep. Prog. Phys. **71**, 016501 (2008).
[55]See Supplemental Material at http://link.aps.org/supplemental/10.1103/PhysRevB.86.085320 for the two references interfaces' cell structures and atomic positions.
[56]A. L. Shluger, K. P. McKenna, P. V. Sushko, D. M. Ramo, and A. V. Kimmel, Modell. Simul. Mater. Sci. Eng. **17**, 084004 (2009).
[57]R. B. Laughlin, Phys. Rev. B **22**, 3021 (1980).
[58]J. D. Dow and D. Redfield, Phys. Rev. B **5**, 594 (1972).
[59]T. Tan, Z. Liu, H. Lu, W. Liu, F. Yan, and W. Zhang, Appl. Phys. A **97**, 475 (2009).
[60]M. C. Cheynet, S. Pokrant, F. D. Tichelaar, and J.-L. Rouvière, J. Appl. Phys. **101**, 054101 (2007).
[61]O. Renault, N. T. Barrett, D. Samour, and S. Quiais-Marthon, Surf. Sci. **566–568**, 526 (2004).
[62]E. Bersch, M. Di, S. Consiglio, R. D. Clark, G. J. Leusink, and A. C. Diebold, J. Appl. Phys. **107**, 043702 (2010).
[63]M. Charbonnier, C. Leroux, V. Cosnier, P. Besson, E. Martinez, N. Benedetto, C. Licitra, N. Rochat, C. Gaumer, K. Kaja *et al.*, IEEE Trans. Electron Devices **57**, 1809 (2010).
[64]T. Nabatame, A. Ohi, and T. Chikyow, *10th IEEE International Conference on Solid-State and Integrated Circuit Technology (ICSICT 2000)* (IEEE, Piscataway, NJ, 2010), pp. 986–989.
[65]K. Kita and A. Toriumi, *IEEE Proc. Intl. Electron Devices Meeting (IEDM 2008)* (IEEE, Piscataway, NJ, 2008), pp. 1–4.
[66]J. Adam and M. D. Rogers, Acta Crystallogr. **12**, 951 (1959).
[67]X. Zhao and D. Vanderbilt, Phys. Rev. B **65**, 233106 (2002).